JOURNAL OF CHEMICAL INFORMATION AND MODELING

Article

pubs.acs.org/jcim

Structural and Dynamic Characterization of Mutated Keap1 for Varied Affinity toward Nrf2: A Molecular Dynamics Simulation Study

I-Chung Cheng,[†] Ya-Jyun Chen,[‡] Chia-Wei Ku,[‡] Yu-Wen Huang,[‡,§] and Chia-Ning Yang*[,‡]

[†]Rehabilitation Division, Zuoying Armed Forces General Hospital, Kaohsiung, Taiwan

[‡]Department of Life Sciences, National University of Kaohsiung, Kaohsiung, Taiwan

Supporting Information

ABSTRACT: Keap1 is an adaptor protein that regulates Nrf2 in response to oxidative stress. Under basal conditions, Nrf2 is negatively regulated through ubiquitination by Keap1. However, upon exposure to oxidative stress, the ubiquitination of Nrf2 is inhibited, resulting in an increased steady-state level of Nrf2 in the nucleus and increased transcription of cytoprotective genes. A gene variant G364C and somatic mutation G430C on Keap1 have recently been reported to substantially impair the Keap1−Nrf2 interaction and to be associated with lung cancer. By contrast, alanine scanning experiments have shown that the mutations S363A, S508A, S555A, and S602A do not affect the ability of Keap1 to bind to Nrf2, regardless of the fact that G364 and G430 are not in contact with Nrf2 whereas the four serine residues are involved in the accommodation of Nrf2 with their hydroxy groups. In this study, molecular dynamics simulations were performed to investigate the structural and dynamic variances among wild-type (WT) Keap1 and the six mutants in unbound form. Principal component analysis of the collected MD trajectories was performed to provide dynamic diversity. Our dynamic and structural observations suggest that the G364C and G430C mutants possess a mobile D385 that moves toward R380, an anchor residue to accommodate an acidic residue in Nrf2, thereby hampering the Keap1−Nrf2 recognition of an electrostatic nature. By contrast, none of the four serine-to-alanine mutants alters the H-bond network formed by the serine backbone to its partner; accordingly, these mutants are almost as intact as the WT structurally and dynamically.

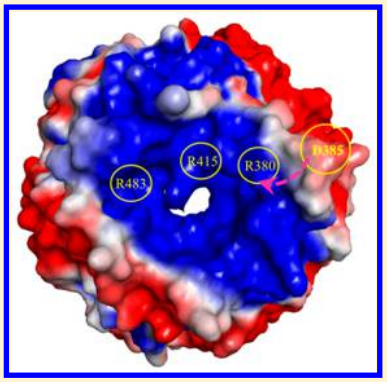

INTRODUCTION

Keap1 is a cysteine-rich protein that represses Nrf2, a basic region leucine zipper (bZIP) transcription factor, to protect cells by regulating a cellular oxidative stress response. Under homeostatic conditions, Keap1 targets Nrf2 for ubiquitin-dependent degradation, thereby suppressing Nrf2-dependent gene expression. When cells are exposed to reactive chemicals or oxidative species that react with Keap1 cysteine residues, Keap1 undergoes a conformational change—although not at the Keap1−Nrf2 interface—that abolishes the Keap1−Nrf2 interaction. Consequently, Nrf2, whose steady-state levels increase, enters the nucleus and activates the antioxidant response element (ARE)-dependent genes.[1−6] Upon recovery of cellular redox homeostasis, Keap1, accompanied by ProTα, travels into the nucleus. Subsequently, the Keap1−Nrf2 complex is transported out of the nucleus by the nuclear export signal in Keap1, causing Nrf2 to degrade in the cytosol.[7−20] On the basis of these mechanisms, targeting Keap1 cystine residues to inhibit Nrf2 degradation and activate ARE gene expression has been a conventional method for chemoprotective agent development.[7,21−25] Recently, Keap1 inhibitors have been designed at the Keap1−Nrf2 interface.[26−32] Therefore, understanding the delicate dynamic and structural variations caused by point mutations on Keap1 at the Keap1−Nrf2 interface shall benefit the development of Keap1 inhibitor design.

Keap1 comprises five characteristic domains: the N-terminal region; the broad complex, tramtrack, bric-a-brac (BTB) region; the intervening region; the double glycine repeat (DGR) or Kelch repeat; and the C-terminal region (CTR).[5,33] Because the DGR and CTR domains form a six-bladed β-propeller structure and are responsible for associating with Nrf2, these domains are denoted as Keap1^{DC} in this study. In the Keap1−Nrf2 complex, two BTB domains are in contact to form a Keap1 homodimer that places two Keap1^{DC} units in an appropriate relative position to recognize Nrf2's evolutionarily conserved ETGE and DLG motifs (hereafter denoted as Nrf2^{ETGE} and Nrf2^{DLG}, respectively). Nrf2^{ETGE} and Nrf2^{DLG} reside in the Neh2 domain of Nrf2 and are 33 amino acids apart. They bind to the same site of Keap1^{DC}; however, the affinity for Keap1^{DC}−Nrf2^{ETGE} is approximately 200-fold higher than that of Keap1^{DC}−Nrf2^{DLG} ($K_a = 2 \times 10^8$ vs 1×10^6).[34] A hinge-and-latch model was proposed by stating that the strongly bound Nrf2^{ETGE} serves as a hinge and binds to Keap1^{DC} at the first place, followed by the weakly bound Nrf2^{DLG}, which plays a decisive role in locking and unlocking Nrf2 from Keap1 for ubiquitination.[35−41] When Keap1^{DC} and Nrf2 are bound through two-site recognition, the 33 amino acid residues between Nrf2^{ETGE} and Nrf2^{DLG}, which are unstruc-

Received: May 21, 2015
Published: September 8, 2015

DOI: 10.1021/acs.jcim.5b00300
J. Chem. Inf. Model. 2015, 55, 2178−2186

tured in the unbound state, can form an α-helix, causing six of the seven lysines to face the same side for efficient ubiquitin recognition.[33,34,37,41−45]

In the six-bladed β-propeller structure of Keap1^{DC}, shown in Figure 1A, each blade is composed of a four-stranded (β1−β4)

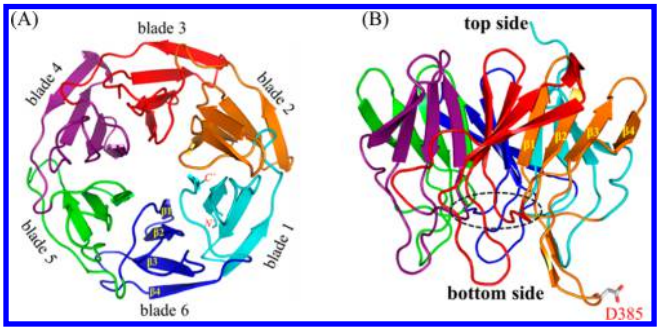

Figure 1. Structure of Keap1^{DC}, which includes the DG and CTR domains. (A) Bottom view of the β-propeller in the ribbon representation. The blades and β strands are labeled. (B) Side view of the β-propeller in the ribbon representation, showing its top and bottom sides. The D385 residue, which will be discussed, is also labeled.

antiparallel β-sheet. Except for blade 1, whose β1 strand prefers to be flanked by solvent and moves too freely to be determined in an X-ray crystallography experiment, each blade's β1 remains the innermost on the central channel of the β-propeller, and the β4 strand remains the outermost. The first 10 amino acid residues in the CTR N-terminus fill in the innermost region of blade 1 and resemble blade 1's β1; hence, the whole β-propeller structure is tightened. The β1−β2 and β3−β4 linkages define the top side of the β-propeller, whereas the β2−β3 and β4−β1 linkages form the bottom side of the β-propeller. As illustrated in the side view in Figure 1B, the β-propeller exhibits a cylindrical shape, where the bottom side is responsible for contacting Nrf2.

Figure 2A shows a structure-based sequence alignment of the six blades in Keap1^{DC}, where some of the conserved residues play crucial roles in strengthening the β-propeller structure. The conserved arginines located in the interblade β4−β1 linkages and the two glycines located in the β2−β3 linkage form a H-bond network to secure two adjacent blades. For instance, R362 in blade 2 uses its side-chain guanidino hydrogen atom and backbone carbonyl oxygen atom to form H-bonds with G378 (the first glycine in the double glycine repeat on blade 2's β2−β3 linkage) and G333 (the second glycine in the double glycine repeat on blade 1's β2−β3 linkage), respectively. Except for R601 and G332, such an H-bond pattern is repeated to maintain inter- and intrablade stability. In this study, we have named this network the RGG ring, as depicted in Figure 2B. Figure 2C shows that the amino acid next to the above-mentioned conserved arginine, positioned as R+1, forms two backbone-to-backbone H-bonds with the amino acid immediately after the double glycine repeat in the same blade. We have termed this network the R+1 H-bond network. For instance, S363 links to R380 in blade 2, and S602 links to Y334 in blade 1. S602 is in the CTR domain that replaces blade 1's β1 strand. Figure 2D shows the R+2 ring that connects each amino acid two positions away from the aforementioned conserved arginine to form a circular H-bond network. This network anchors the six blades for a stable β-propeller structure. Moreover, the conserved tyrosines and tryptophans spreading in β2, β3, and β4 contribute π−π interactions; each of the aforementioned conserved arginines forms a salt bridge with an acidic amino acid residue in β3 within the same blade.

Recently, two single-point mutations in Keap1^{DC}, G364C and G430C, have been found to reduce the Keap1−Nrf2 interaction, resulting in enhanced Nrf2 transactivational activity.[33,46] G364C is a somatic mutation found in human lung cancer patients, whereas G430C is a homozygous mutation found in a lung adenocarcinoma-derived cell line.[33,47] The abolishment of the Keap1−Nrf2 interaction caused by these two mutations has been proven in experimental observations, and although possible structural mechanisms have been proposed,[33,48] solid evidence remains lacking. In addition, in an alanine-scan mutagenesis series on Keap1^{DC} performed to identify the contributions to Keap1^{DC}−Nrf2 affinity, point mutations on R380, R415, and R483, which are essential for recognizing the negatively charged amino acid residues of Nrf2^{ETGE} and Nrf2^{DLG}, were observed to enhance the Nrf2-dependent gene expression, whereas the S363A, S508A, S555A, and S602A mutants showed no significant reduction in Keap1−Nrf2 affinity.[49] Structural investigations of the Keap1^{DC}−Nrf2^{ETGE} and Keap1^{DC}−Nrf2^{DLG} complexes (Figures S1 and S2) concluded that Keap1^{DC} uses R380, R415, and R483 to provide electrostatic interactions, Y334, Y525, and Y572 to provide hydrophobic interactions, and S363, S508, S555, and S602 to provide H-bonds to Nrf2^{ETGE} and Nrf2^{DLG}. Interestingly, G364 and G430 are not involved in the complex formation, but their mutation results in abolished affinity. On the other hand, although S363, S508, S555, and S602 are at the peptide binding interface, replacement of any one of them by alanine does not affect the binding affinity.[49,50]

In this work, molecular dynamics (MD) simulations of free wild-type (WT) Keap1^{DC} and its G364C, G430C, S363A, S508A, S555A, and S602A mutants, instead of the Keap1^{DC}−Nrf2^{ETGE} or Keap1^{DC}−Nrf2^{DLG} complex, were performed to investigate their dynamic and conformational variances leading to different affinities toward Nrf2. It is notable that G364 is part of the R+2 ring (Figure 2D) and G430 is located in the RGG ring (Figure 2B), whereas S363, S508, S555, and S602 are involved in the R+1 H-bond network (Figure 2C). Using snapshots collected from the MD simulation trajectories, principal component analyis (PCA) was applied to shed light on the dynamic discrepancy among the seven studied systems. Our observations provide evidence that the G364C and G430C mutants exhibit a different dynamic behavior that hampers Keap1^{DC}−Nrf2 association, which greatly relies on long-range electrostatic attractions.

MATERIALS AND METHODS

System Setup. MD simulations were performed to compare the dynamics and structures of WT Keap1^{DC} and its G430C, G364C, S363A, S508A, S555A, and S602A mutants (MTs) to reveal the unbinding behavior caused by the G364C and G430C mutations. The coordinates for human Keap1 determined by X-ray crystallography (PDB entry 1u6d)[51] were applied to obtain the initial WT structure, and the six MTs were generated by manually replacing the indicated amino acid residue. The N- and C-termini of the WT and MTs were capped by acetyl and *N*-methyl groups, respectively. Each Keap1^{DC} was immersed in a cubic box of TIP3P waters.[52,53] An appropriate size of the box was selected to ensure that the distance between the atoms in each Keap1^{DC} and the wall was

DOI: 10.1021/acs.jcim.5b00300
J. Chem. Inf. Model. 2015, 55, 2178−2186

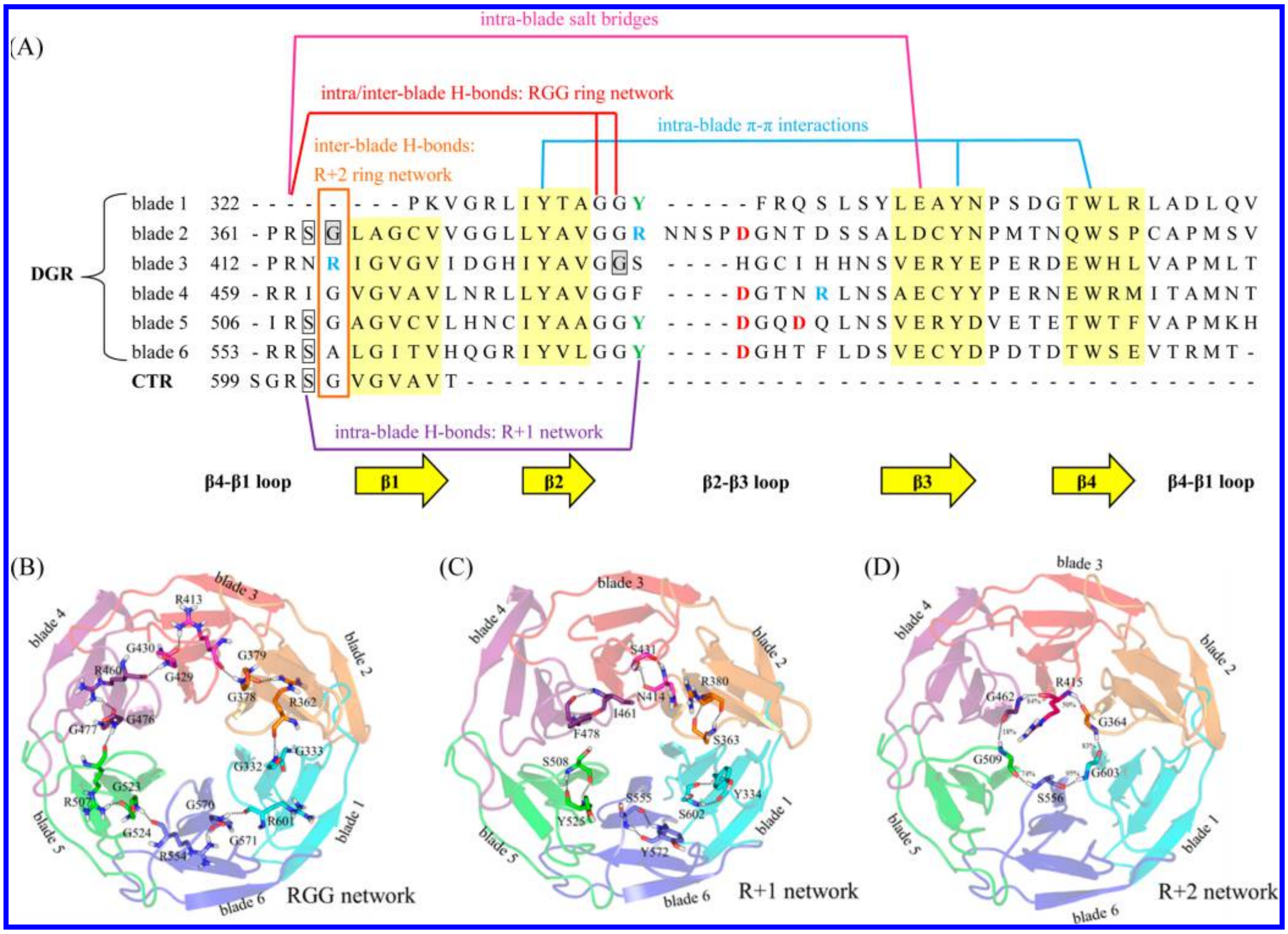

Figure 2. (A) Structure-based sequence alignment for the six blades in Keap1[DC]. The four β strands in each blade are presented with a yellow background. Mutation sites G364 and G430, whose replacement by cysteine abolishes the Keap1−Nrf2 affinity, are boxed and shown with a gray background. Mutation sites S363, S508, S555, and S602, whose replacement by alanine does not affect the Keap1−Nrf2 affinity, are boxed. Several inter- and intrablade interactions to maintain the β-propeller structure are specified. R380, R415, and R483, which provide electrostatic interactions toward Nrf2, are colored cyan, whereas Y334, Y525, and Y572, which provide hydrophobic interactions upon Nrf2 binding, are colored green. D385, D479, D526, D529, and D573, whose movement may be influential in Keap1−Nrf2 recognition, are colored red. (B) The RGG H-bond network. (C) The R+1 H-bond network. (D) The R+2 H-bond network.

greater than 12 Å. For all of the systems, including the WT and MTs, seven Na^+ ions were included for electrical neutralization. The neighboring TIP3P water molecules within 1.5 Å of the complex were removed to prevent unnecessary H-bonds between the studied Keap1[DC] and the added solvent molecules at the beginning of the simulation. Each solvated system was energy-minimized by considering three stages, each employing 500 steps of the steepest-descent algorithm and 500 steps of the conjugate-gradient algorithm with a nonbonded cutoff of 8.0 Å. In stage 1, the Keap1[DC] structure was restrained so that the added TIP3P water molecules could reorient properly in the presence of Keap1[DC]. In stage 2, the backbone of Keap1[DC] was restrained so that the amino acid side chains could find appropriate ways to avoid neighboring specious conflicts, particularly for the six MTs. In stage 3, the entire solvated system was minimized without any restraints.

Molecular Dynamics Simulations. The MD simulations using Amber 12 and the ff99sb force field were performed according to the standard protocol, which entails gradual heating, density, equilibration, and production procedures in the isothermal isobaric (*NPT*) ensemble (P = 1 atm and T = 300 K). A minimized solvated system was used as the starting structure for subsequent MD simulations. In the 500 ps heating procedure, the system was gradually heated from 0 to 300 K in 50 ps, followed by density at 300 K for 500 ps and constant equilibration at 300 K for 50 ps. After the equilibration procedure, the system underwent a 30 ns production procedure for conformation collection. The time step was set at 2 fs. A snapshot was captured every 10 ps to record the conformation trajectory during production MD. An 8 Å cutoff was applied to treat nonbonding interactions, such as short-range electrostatics and van der Waals interactions, whereas the particle-mesh Ewald method was applied to treat long-range electrostatic interactions.[54] The SHAKE algorithm[55,56] was used to constrain all of the bonds containing hydrogen atoms to their equilibrium lengths. For structural and energetic analysis, we used the final 15 ns of the trajectory, which covered 150 conformation snapshots for each complex system.

Principal Component Analysis. To characterize the dynamic variation between the WT and the six MTs, we performed PCA to investigate the MD trajectories collected between 15 and 30 ns. PCA is an effective tool for investigating the recorded motion of each atom in a reduced-dimension manner and represents the trajectories in several combinational

DOI: 10.1021/acs.jcim.5b00300
J. Chem. Inf. Model. 2015, 55, 2178−2186

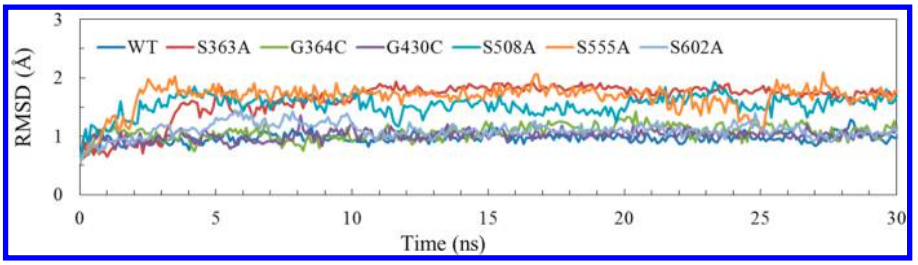

Figure 3. Time evolution of the Cα RMSDs for the WT and six MTs.

modes by separating large collective motions from random thermal fluctuations.[57,58] In short, PCA is based on the covariance matrix

$$\mathrm{Cov}(i, j) = \langle (\mathbf{r}_i(t) - \langle \mathbf{r}_i \rangle_t) \cdot (\mathbf{r}_j(t) - \langle \mathbf{r}_j \rangle_t) \rangle_t$$

where $\mathbf{r}_i$ and $\mathbf{r}_j$ are the Cartesian coordinates of atoms i and j, respectively, and $\langle \mathbf{r} \rangle_t$ is the average of the variable over duration t in the collected MD trajectory. The eigenvectors and eigenvalues of this matrix represent the collective dynamic modes and amplitudes, respectively. We used the ProDy program[59−61] to conduct the PCA.

RESULTS AND DISCUSSION

MD Stability of WT Keap1^{DC} and the MTs. The Cα root-mean-square deviation (RMSD) values for the WT and six MTs in the production duration as functions of time were plotted to evaluate the quality and convergence of the MD trajectories (Figure 3). The S508A and S555A curves experienced some minor fluctuations, whereas the WT, G364C, and G430C curves became stable after 5 ns and the S363A and S602A curves became stable after 10 ns. For each MD system, 150 snapshots taken at equal time intervals between 15 and 30 ns were captured for dynamic and structural analyses to explain the binding and unbinding behaviors of the WT and MTs for Keap1^{DC}−Nrf2.

Dynamic Discrepancy. PCA of the MD trajectories collected between 15 and 30 ns was conducted to quantize the essential dynamic modes of motion that may cause the different Keap1^{DC}−Nrf2 binding behaviors observed in previous biomolecular experiments.[33,49] The first PCA modes were found to account for 81%, 63%, 74%, 63%, 74%, 67%, and 67% of the total variance for the WT and the G364C, G430C, S363A, S508A, S555A, and S602A MTs, respectively. The PC1 motion of the WT (left panel in Figure 4A) is a "breathing" mode with the β2−β3 linkages of the six blades moving inward and outward relative to the cylinder center. The PC1 motions of the six MTs also display a similar breathing mode but with pronounced motion in blade 2's β2−β3 linkage (left panels in Figure 4B−G). Moreover, in G430C the mobility of blade 4's β2−β3 linkage is comparable to that in blade 2. As the side view of Keap1^{DC} in Figure 1B indicates, the conformational flexibility among the six β2−β3 linkages may be influential in Keap1^{DC}−Nrf2 recognition since the binding pocket (circled by the black dashed line) is in a basin surrounded by these six β2−β3 linkages.

As a further test, we analyzed the 15−30 ns trajectories of D385, D479, D526, D529, and D573 because they are located on the β2−β3 linkage tips of blades 2, 4, 5, and 6 and their negatively charged carboxylate groups would be influential in Keap1^{DC}−Nrf2 recognition through electrostatic attractions. As shown in the middle panel in Figure 4A, the trajectories of these five aspartate residues in the WT show local vibrations since the WT's PC1 is not in great magnitude compared with those of the six MTs. Also provided in this figure are the trajectories of R380, R415, and R483 (in the line representation) collected in the MD simulation for unbound Keap1^{DC} alongside the superposition of Y334, Y525, Y572, R380, R415, and R483 (in the stick representation) in the Keap1^{DC}−Nrf2^{ETGE} complex (PDB entry 2flu), where the backbone of Nrf2^{ETGE} and its key residues E79′ and E82′ are also specified. It is notable that R380 and R415 in the unbound form of Keap1^{DC} are anchor residues that are ready to recognize E82′ and E79′ of Nrf2^{ETGE}. R483 is oriented toward the solvent in the unbound form and gets induced to the bound-form position when R380−E82′ and R415−E79′ interactions form in the first place. Y334, Y525, and Y572 are on the other side of Nrf2^{ETGE} for hydrophobic interactions to complete the binding pocket.

In comparison with WT Keap1^{DC}, the trajectory of the G364C mutant's D385 (middle panel in Figure 4B) moves back and forth in the region above R380 in a greater magnitude (right panel in Figure 4B) to correlate with the dramatic PC1 motion of blade 2's β2−β3 linkage (left panel in Figure 4B). We believe that this movement directly disrupts the R380−E82′ interaction and consequently indirectly affects the R415−E79′ interaction and the reorientation of R483 for the R483−E79′ interaction. The D385 trajectory in the G430C mutant also adopts the same behavior as in the G364C MT, and the D475 trajectory is more flexible (middle panel in Figure 4C) in comparison with the other studied systems, whose blade 4 β2−β3 linkages are somewhat stable. On the contrary, the D385 trajectories for the S363A, S508A, S555A, and S602A MTs (middle and right panels of Figure 4D−G) do not show the tendency observed for G364C and G430C to move toward the region above R380, and accordingly, these four MTs still hold affinity toward Nrf2.

Structural Characterization. As shown in Figure 2C, S363, S508, S555, and S602 use their backbone carbonyl oxygen and amino hydrogen atoms to link to their partners in the R+1 H-bond network (R380, Y525, Y572, and Y334, respectively). Accordingly, this explains why replacement of S363, S508, S555, and S602 by alanine did not result in a significant affinity reduction between Keap1^{DC} and Nrf2, as the smaller alanine residue would only bring minor steric collapse for the nearby amino acid residues but not disrupt the H-bond network involving the key residues interacting with Nrf2. As shown in Figures S1 and S2, where these serines use their side-chain hydroxyl group to interact with Nrf2^{DLG} and Nrf2^{ETGE}, apparently a shortage of one H-bond does not impair the complex formation because numerous electrostatic interactions involving R380, R415, and R483 maintain the binding.

Figure 5A presents the aforementioned stabilization contributed by the H-bond networks composed of the RGG,

DOI: 10.1021/acs.jcim.5b00300
J. Chem. Inf. Model. 2015, 55, 2178−2186

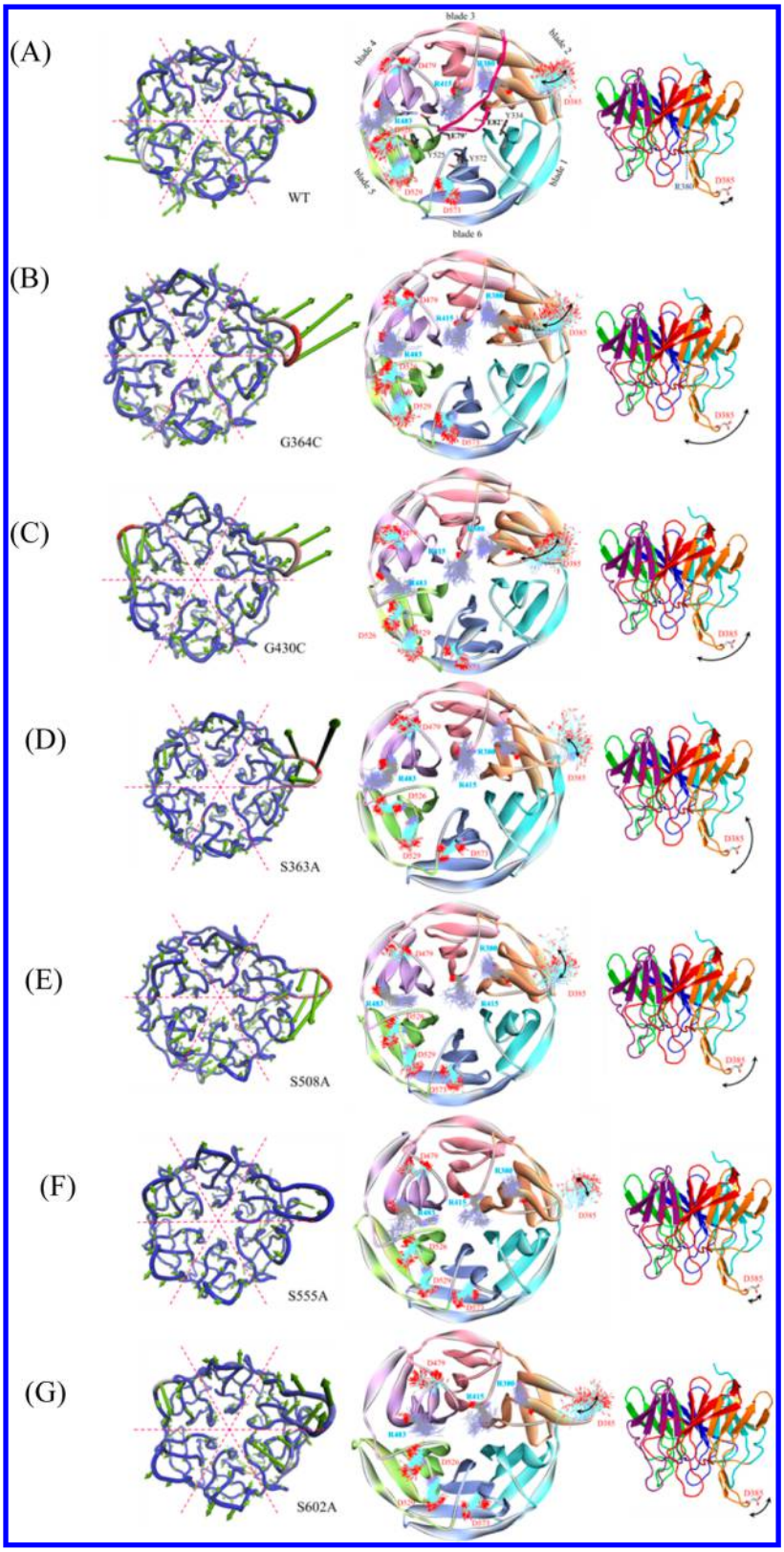

Figure 4. Left panels: PC1 data, where the color code for high to low mobility is red to white to blue. Middle panels: trajectories of negatively charged residues surrounding the binding pocket. Right panels: motion of D385 and its magnitude. (A) WT; (B) G364C; (C) G430C; (D) S363A; (E) S508A; (F) S555A; (G) S602A.

R+1, and R+2 rings in addition to the salt bridges formed between the conserved R of the $\beta4-\beta1$ linkage and the conserved D/E of blade 3 in the WT. Despite the missing R601−G332 H-bond, these networks are quite symmetric. Moreover, except for the low occupancies of the G364−R415 and G462−S509 H-bonds, suggesting that the R+2 ring is vulnerable to structural instability, all of the marked interactions occurred with 100% occupancies in the analyzed MD duration.

DOI: 10.1021/acs.jcim.5b00300
J. Chem. Inf. Model. 2015, 55, 2178−2186

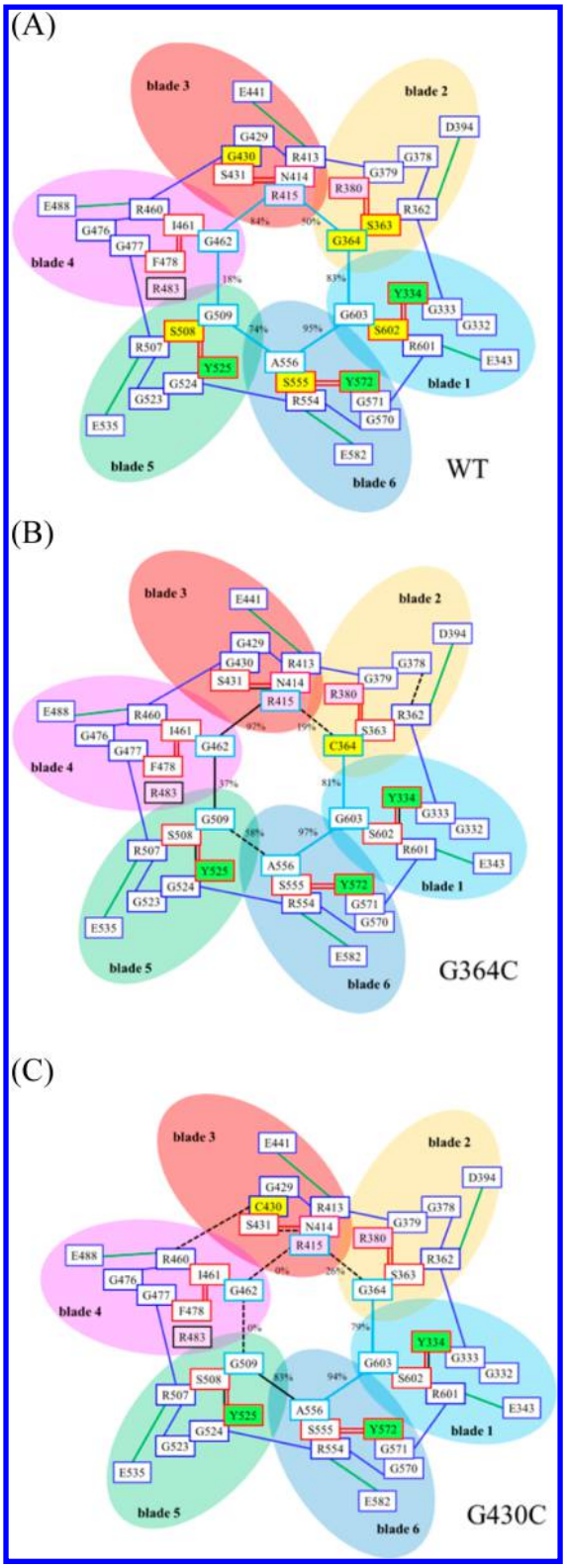

Figure 5. H-bond networks influencing the stability of the bottom side of Keap1^{DC} in (A) WT, (B) G364C, and (C) G430C. Dashed lines represent the weakened H-bonds in comparison with those in the WT.

In regard to the G364C mutant, the mutated G364 is a member of the R+2 H-bond network, and our structural analysis indicates that the slightly bulker C364 has a structural influence on the R+2 ring H-bond network. In other words, the C364−R415 H-bond is weakened, resulting in stronger R415-G462 and G462-S509 H-bonds, as shown in Figure 5B.

Compared with G364C, the structural influence of the G430C mutation is stronger. As shown in Figure 5C, our H-bond analysis revealed that one of the two N414−S431 H-bonds in the R+1 network does not exist and that the R415−G462−G509 H-bond breakage destroys part of the R+2 ring network and reduces the occupancy of the C430−R460 H-bond in the RGG ring network. Triggered by the replacement of G430 with the bulkier C430, all of these changes cause blade 4 to move toward blade 5.

Correlation between Dynamic and Structural Observations. To link the dynamic discrepancy determined by the PC1 mode and the structural influence caused by the G364C and G430C mutations, we focused on the H-bonds related to blade 2's β2−β3 linkage, which is composed of two antiparallel β-strands, as depicted in Figure 6. The first strand, adjacent to blade 2's β2, faces the center of the Keap1^{DC} propeller, whereas the second strand, adjacent to blade 2's β3, faces the solvent. The rocking motion is related to the interplay of the first β-strand with the other amino acid residues. On the basis of our analysis, G379 (the second amino acid residue in the first β strand) and R362 (which is linked to G379 based on the RGG network) play pivotal roles. As shown in Figure 6A for the WT, numerous hydrogen atoms of the R362 guanidino group are secured by the carboxylic acid oxygen atom of D394 (the second amino acid residue in blade 2's β3 and close to the end of the second β-strand) and the carbonyl oxygen atoms of G378 and V360. Conversely, the backbone carbonyl oxygen atom of R362 is secured by G333 through the RGG network. Overall, R362, G378, D394, and V360 in the WT stabilize blade 2's β2−β3 linkage, enabling a rocking motion of minor magnitude. As shown in Figure 6B, C, the H-bond networks in the G364C and G430C mutants are partially affected as mentioned above: the V360−R362 H-bond vanishes, and the R362 side chain frees blade 2's β2−β3 linkage to move between the solvent and the propeller center with a greater magnitude. The V360−R362 H-bond occupancy analysis indicated 70% occupancy for S363A, 0% for S508A and S555A, and 39% for S602A, which are consistent with the PCA data shown in Figure 4D−G. In other words, in the S363A mutant, the R362 motion remains dependent on V360, and thus, blade 2's β2−β3 linkage therein shows a minor rocking motion. By contrast, R362 in the S508A, S555A, and S602A MTs is not attached to V360, and therefore, the rocking motion was apparently obvious.

CONCLUSION

In this study, we conducted a series of MD simulations of WT Keap1^{DC} and six MTs to elucidate the unbinding behavior of the G364C and G430C MTs and provide a rationale to explain why S363A, S508A, S555A, and S603A MTs retain affinity toward Nrf2. We used the unbound forms of the WT and MTs instead of the Keap1^{DC}−Nrf2^{ETGE} or Keap1^{DC}−Nrf2^{DLG} complex for discussion because the Nrf2^{ETGE} and Nrf2^{DLG} peptides exhibit a rigid hairpin conformation maintained by H-bonds and because these peptides are associated with Keap1^{DC} on the basis of several strong electrostatic interactions. In our unpublished simulations, structures with a mutated Keap1^{DC} bound with Nrf2^{ETGE} and Nrf2^{DLG} remained considerably stable. Therefore, discussing their unbinding behaviors would be difficult, particularly for G364C and G430C, which are not at the binding interface.

DOI: 10.1021/acs.jcim.5b00300
J. Chem. Inf. Model. 2015, 55, 2178−2186

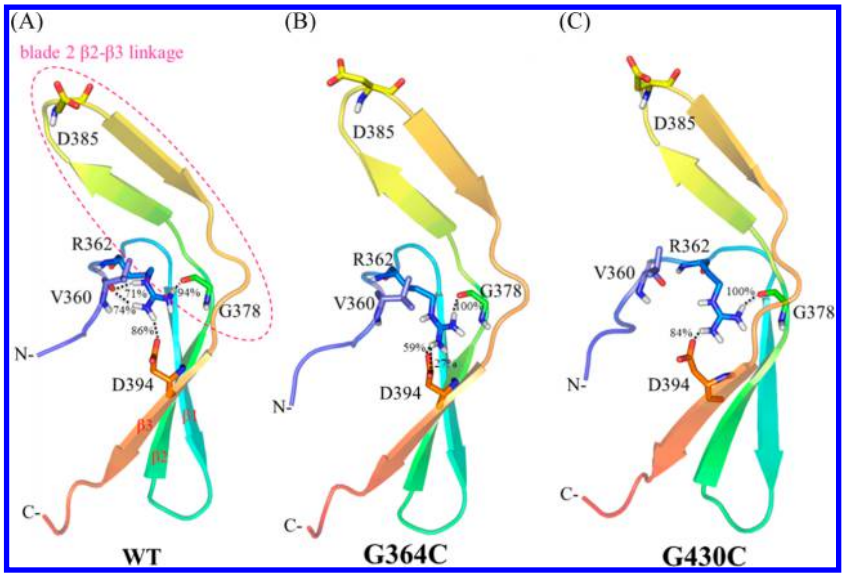

Figure 6. H-bonds to stabilize blade 2's $\beta2-\beta3$ linkage in (A) WT, (B) G364C, and (C) G430C.

The reason that the S363A, S508A, S555A, and S602A MTs maintain their affinity to Nrf2 regardless of their involvement at the Keap1^{DC}–Nrf2 interface is that these serines use their backbone atoms to participate in the R+1 H-bond network (Figure 2C); therefore, replacing one of them with an alanine residue does not severely impair the R+1 network. The importance of the R+1 network is to hold R380 (by S363), Y334 (by S602), Y525 (by S508), and Y572 (by S555) in appropriate positions to accommodate Nrf2. G364 is part of the R+2 ring (Figure 2D). Its replacement by the slightly bulkier C364 alters the stability of the R+2 ring and causes R362 to detach from V360 and the magnitude of the rocking motion of blade 2's $\beta2-\beta3$ linkage to increase (Figure 4B). G430 is part of the RGG network (Figure 2B). Its replacement by C430 introduces instability in the RGG, R+1, and R+2 networks (Figure 5C). Moreover, the influences on the R+2 network bring disorder on G364, indirectly detach R362 from V360, and enhance the rocking motion of blade 2's $\beta2-\beta3$ linkage (Figure 4C). Moreover, PCA data indicate that the G364C and G430C mutants exhibit a rocking motion of blade 2's $\beta2-\beta3$ linkage to expand and contract the entrance fpr the incoming Nrf2^{ETGE} and Nrf2^{DLG}, as evidenced by the D385 trajectories (Figure 4B,C). In summary, this work highlights the important observation that dynamic and structural alterations derived from point mutations, especially of residues not in the binding pocket, are essential in varying protein–protein recognition.

■ ASSOCIATED CONTENT

Supporting Information

The Supporting Information is available free of charge on the ACS Publications website at DOI: 10.1021/acs.jcim.5b00300.

Interactions of Keap1^{DC}–Nrf2^{DLG} determined using the X-ray crystallographic structures for mice (PDB entry 2dyh) and humans (PDB entry 2flu) (PDF)

■ AUTHOR INFORMATION

Corresponding Author

*Tel: 886-7-5919717. Fax: 886-75919404. E-mail: cnyang@nuk.edu.tw. Address: No. 700 Kaohsiung University Road, Nan-Tzu District 811, Kaohsiung, Taiwan.

Present Address

§Y.-W.H.: Institute of Bioinformatics and Systems Biology, National Chiao Tung University, Hsinchu, Taiwan.

Notes

The authors declare no competing financial interest.

■ ACKNOWLEDGMENTS

The authors gratefully acknowledge the financial support provided for this study by Zuoying Armed Forces General Hospital (Kaohsiung, Taiwan) under Grant ZBH 103-17.

■ REFERENCES

(1) Nguyen, T.; Nioi, P.; Pickett, C. B. The Nrf2-Antioxidant Response Element Signaling Pathway and its Activation by Oxidative Stress. *J. Biol. Chem.* **2009**, *284*, 13291–13295.

(2) Sun, Z.; Zhang, S.; Chan, J. Y.; Zhang, D. D. Keap1 Controls Postinduction Repression of the Nrf2-Mediated Antioxidant Response by Escorting Nuclear Export Of Nrf2. *Mol. Cell. Biol.* **2007**, *27*, 6334–6349.

(3) Stewart, D.; Killeen, E.; Naquin, R.; Alam, S.; Alam, J. Degradation of Transcription Factor Nrf2 via the Ubiquitin-Proteasome Pathway and Stabilization by Cadmium. *J. Biol. Chem.* **2003**, *278*, 2396–2402.

(4) Nguyen, T.; Sherratt, P. J.; Huang, H.-C.; Yang, C. S.; Pickett, C. B. Increased Protein Stability as a Mechanism that Enhances Nrf2-Mediated Transcriptional Activation of the Antioxidant Response Element Degradation of Nrf2 by the 26 S Proteasome. *J. Biol. Chem.* **2003**, *278*, 4536–4541.

(5) Itoh, K.; Wakabayashi, N.; Katoh, Y.; Ishii, T.; Igarashi, K.; Engel, J. D.; Yamamoto, M. Keap1 Represses Nuclear Activation of Antioxidant Responsive Elements By Nrf2 through Binding to the Amino-Terminal Neh2 Domain. *Genes Dev.* **1999**, *13*, 76–86.

(6) Itoh, K.; Chiba, T.; Takahashi, S.; Ishii, T.; Igarashi, K.; Katoh, Y.; Oyake, T.; Hayashi, N.; Satoh, K.; Hatayama, I.; Yamamoto, M.; Nabeshima, Y.-i. An Nrf2/Small Maf Heterodimer Mediates the Induction of Phase II Detoxifying Enzyme Genes through Antioxidant Response Elements. *Biochem. Biophys. Res. Commun.* **1997**, *236*, 313–322.

(7) Zhang, D. D.; Hannink, M. Distinct cysteine residues in Keap1 are Required for Keap1-Dependent Ubiquitination of Nrf2 and for Stabilization Of Nrf2 by Chemopreventive Agents and Oxidative Stress. *Mol. Cell. Biol.* **2003**, *23*, 8137–8151.

(8) Dhakshinamoorthy, S.; Jain, A. K.; Bloom, D. A.; Jaiswal, A. K. Bach1 Competes with Nrf2 Leading to Negative Regulation of the

DOI: 10.1021/acs.jcim.5b00300
J. Chem. Inf. Model. 2015, 55, 2178–2186

Antioxidant Response Element (ARE)-Mediated NAD (P) H: Quinone Oxidoreductase 1 Gene Expression and Induction in Response to Antioxidants. *J. Biol. Chem.* **2005**, *280*, 16891−16900.
(9) Jain, A. K.; Jaiswal, A. K. Phosphorylation of Tyrosine 568 Controls Nuclear Export of Nrf2. *J. Biol. Chem.* **2006**, *281*, 12132−12142.
(10) Jain, A. K.; Jaiswal, A. K. GSK-3beta Acts Upstream of Fyn Kinase in Regulation of Nuclear Export and Degradation of NF-E2 Related Factor 2. *J. Biol. Chem.* **2007**, *282*, 16502−10.
(11) Kaspar, J. W.; Niture, S. K.; Jaiswal, A. K. Nrf2: INrf2 (Keap1) Signaling in Oxidative Stress. *Free Radical Biol. Med.* **2009**, *47*, 1304−1309.
(12) Niture, S. K.; Jain, A. K.; Jaiswal, A. K. Antioxidant-induced Modification of INrf2 Cysteine 151 and PKC-δ-mediated Phosphorylation of Nrf2 Serine 40 are Both Required for Stabilization and Nuclear Translocation of Nrf2 and Increased Drug Resistance. *J. Cell Sci.* **2009**, *122*, 4452−4464.
(13) Niture, S. K.; Jaiswal, A. K. Prothymosin-α mediates Nuclear Import of the INrf2/Cul3·Rbx1 Complex to Degrade Nuclear Nrf2. *J. Biol. Chem.* **2009**, *284*, 13856−13868.
(14) Kaspar, J. W.; Jaiswal, A. K. Antioxidant-induced Phosphorylation of Tyrosine 486 Leads to Rapid Nuclear Export of Bach1 that Allows Nrf2 to Bind to the Antioxidant Response Element and Activate Defensive Gene Expression. *J. Biol. Chem.* **2010**, *285*, 153−162.
(15) Kaspar, J. W.; Jaiswal, A. K. Tyrosine Phosphorylation Controls Nuclear Export of Fyn, Allowing Nrf2 Activation of Cytoprotective Gene Expression. *FASEB J.* **2011**, *25*, 1076−1087.
(16) Niture, S. K.; Jain, A. K.; Shelton, P. M.; Jaiswal, A. K. Src Subfamily Kinases Regulate Nuclear Export and Degradation of Transcription Factor Nrf2 to Switch off Nrf2-Mediated Antioxidant Activation of Cytoprotective Gene Expression. *J. Biol. Chem.* **2011**, *286*, 28821−28832.
(17) Rada, P.; Rojo, A. I.; Chowdhry, S.; McMahon, M.; Hayes, J. D.; Cuadrado, A. SCF/β-TrCP Promotes Glycogen Synthase Kinase 3-Dependent Degradation of the Nrf2 Transcription Factor in a Keap1-Independent Manner. *Mol. Cell. Biol.* **2011**, *31*, 1121−1133.
(18) Kaspar, J. W.; Niture, S. K.; Jaiswal, A. K. Antioxidant-Induced INrf2 (Keap1) Tyrosine 85 Phosphorylation Controls The Nuclear Export and Degradation of the INrf2-Cul3-Rbx1 Complex to Allow Normal Nrf2 Activation and Repression. *J. Cell Sci.* **2012**, *125*, 1027−1038.
(19) Shelton, P.; Jaiswal, A. K. The Transcription Factor NF-E2-Related Factor 2 (Nrf2): a Protooncogene? *FASEB J.* **2013**, *27*, 414−423.
(20) Niture, S. K.; Khatri, R.; Jaiswal, A. K. Regulation of Nrf2—an Update. *Free Radical Biol. Med.* **2014**, *66*, 36−44.
(21) Dinkova-Kostova, A. T.; Massiah, M. A.; Bozak, R. E.; Hicks, R. J.; Talalay, P. Potency of Michael Reaction Acceptors as Inducers of Enzymes that Protect Against Carcinogenesis Depends on their Reactivity with Sulfhydryl Groups. *Proc. Natl. Acad. Sci. U. S. A.* **2001**, *98*, 3404−3409.
(22) Dinkova-Kostova, A. T.; Holtzclaw, W. D.; Cole, R. N.; Itoh, K.; Wakabayashi, N.; Katoh, Y.; Yamamoto, M.; Talalay, P. Direct Evidence that Sulfhydryl Groups of Keap1 Are the Sensors Regulating Induction of Phase 2 Enzymes that Protect Against Carcinogens and Oxidants. *Proc. Natl. Acad. Sci. U. S. A.* **2002**, *99*, 11908−11913.
(23) Hong, F.; Freeman, M. L.; Liebler, D. C. Identification of Sensor Cysteines in Human Keap1Modified by the Cancer Chemopreventive Agent Sulforaphane. *Chem. Res. Toxicol.* **2005**, *18*, 1917−1926.
(24) Holland, R.; Hawkins, A. E.; Eggler, A. L.; Mesecar, A. D.; Fabris, D.; Fishbein, J. C. Prospective Type 1 and Type 2 Disulfides of Keap1 Protein. *Chem. Res. Toxicol.* **2008**, *21*, 2051−2060.
(25) Kensler, T. W.; Wakabayashi, N. Nrf2: Friend or Foe for Chemoprevention? *Carcinogenesis* **2010**, *31*, 90−99.
(26) Dhakshinamoorthy, S.; Jaiswal, A. K. Functional Characterization and Role of INrf2 in Antioxidant Response Element-Mediated Expression and Antioxidant Induction of NAD(P)H: Quinone Oxidoreductasel Gene. *Oncogene* **2001**, *20*, 3906−3917.
(27) Miyata, T.; Kikuchi, K.; Kiyomoto, H.; van Ypersele de Strihou, C. New Era for Drug Discovery and Development in Renal Disease. *Nat. Rev. Nephrol.* **2011**, *7*, 469−477.
(28) Hancock, R.; Bertrand, H. C.; Tsujita, T.; Naz, S.; El-Bakry, A.; Laoruchupong, J.; Hayes, J. D.; Wells, G. Peptide Inhibitors of the Keap1−Nrf2 Protein−Protein Interaction. *Free Radical Biol. Med.* **2012**, *52*, 444−451.
(29) Magesh, S.; Chen, Y.; Hu, L. Small Molecule Modulators of Keap1−Nrf2-ARE Pathway as Potential Preventive and Therapeutic Agents. *Med. Res. Rev.* **2012**, *32*, 687−726.
(30) Jiang, Z.-Y.; Lu, M.-C.; Xu, L. L.; Yang, T.-T.; Xi, M.-Y.; Xu, X.-L.; Guo, X.-K.; Zhang, X.-J.; You, Q.-D.; Sun, H.-P. Discovery of Potent Keap1−Nrf2 Protein−Protein Interaction Inhibitor Based on Molecular Binding Determinants Analysis. *J. Med. Chem.* **2014**, *57*, 2736−2745.
(31) Li, C.; Xu, X.; Wang, X. J.; Pan, Y. Imine Resveratrol Analogues: Molecular Design, Nrf2 Activation and SAR Analysis. *PLoS One* **2014**, *9*, e101455.
(32) Zhuang, C.; Narayanapillai, S.; Zhang, W.; Sham, Y. Y.; Xing, C. Rapid Identification of Keap1−Nrf2 Small-Molecule Inhibitors through Structure-Based Virtual Screening and Hit-Based Substructure Search. *J. Med. Chem.* **2014**, *57*, 1121−1126.
(33) Padmanabhan, B.; Tong, K. I.; Ohta, T.; Nakamura, Y.; Scharlock, M.; Ohtsuji, M.; Kang, M.-I.; Kobayashi, A.; Yokoyama, S.; Yamamoto, M. Structural Basis For Defects of Keap1 Activity Provoked by its Point Mutations in Lung Cancer. *Mol. Cell* **2006**, *21*, 689−700.
(34) Tong, K. I.; Katoh, Y.; Kusunoki, H.; Itoh, K.; Tanaka, T.; Yamamoto, M. Keap1 recruits Neh2 through Binding to ETGE and DLG Motifs: Characterization of the Two-Site Molecular Recognition Model. *Mol. Cell. Biol.* **2006**, *26*, 2887−2900.
(35) Mitsuishi, Y.; Motohashi, H.; Yamamoto, M. The Keap1−Nrf2 System In Cancers: Stress Response and Anabolic Metabolism. *Front. Oncol.* **2012**, *2*, 200.
(36) Taguchi, K.; Motohashi, H.; Yamamoto, M. Molecular Mechanisms of the Keap1−Nrf2 Pathway in Stress Response and Cancer Evolution. *Genes Cells* **2011**, *16*, 123−140.
(37) Shibata, T.; Ohta, T.; Tong, K. I.; Kokubu, A.; Odogawa, R.; Tsuta, K.; Asamura, H.; Yamamoto, M.; Hirohashi, S. Cancer Related Mutations in NRF2 Impair its Recognition by Keap1-Cul3 E3 Ligase and Promote Malignancy. *Proc. Natl. Acad. Sci. U. S. A.* **2008**, *105*, 13568−13573.
(38) Watai, Y.; Kobayashi, A.; Nagase, H.; Mizukami, M.; McEvoy, J.; Singer, J. D.; Itoh, K.; Yamamoto, M. Subcellular Localization and Cytoplasmic Complex Status of Endogenous Keap1. *Genes Cells* **2007**, *12*, 1163−1178.
(39) Tong, K. I.; Padmanabhan, B.; Kobayashi, A.; Shang, C.; Hirotsu, Y.; Yokoyama, S.; Yamamoto, M. Different Electrostatic Potentials Define ETGE and DLG Motifs as Hinge and Latch in Oxidative Stress Response. *Mol. Cell. Biol.* **2007**, *27*, 7511−7521.
(40) Tong, K. I.; Kobayashi, A.; Katsuoka, F.; Yamamoto, M. Two-Site Substrate Recognition Model for the Keap1−Nrf2 System: a Hinge and Latch Mechanism. *Biol. Chem.* **2006**, *387*, 1311−1320.
(41) McMahon, M.; Thomas, N.; Itoh, K.; Yamamoto, M.; Hayes, J. D. Dimerization of Substrate Adaptors can Facilitate Cullin-Mediated Ubiquitylation of Proteins by a "Tethering" Mechanism a Two-Site Interaction Model for the Nrf2-Keap1 Complex. *J. Biol. Chem.* **2006**, *281*, 24756−24768.
(42) Behrends, C.; Harper, J. W. Constructing and Decoding Unconventional Ubiquitin Chains. *Nat. Struct. Mol. Biol.* **2011**, *18*, 520−528.
(43) Komander, D. The Emerging Complexity of Protein Ubiquitination. *Biochem. Soc. Trans.* **2009**, *37*, 937−953.
(44) Zhang, D. D.; Lo, S.-C.; Cross, J. V.; Templeton, D. J.; Hannink, M. Keap1 Is a Redox-Regulated Substrate Adaptor Protein for a Cul3-Dependent Ubiquitin Ligase Complex. *Mol. Cell. Biol.* **2004**, *24*, 10941−10953.
(45) Wakabayashi, N.; Dinkova-Kostova, A. T.; Holtzclaw, W. D.; Kang, M.-I.; Kobayashi, A.; Yamamoto, M.; Kensler, T. W.; Talalay, P.

DOI: 10.1021/acs.jcim.5b00300
J. Chem. Inf. Model. 2015, 55, 2178−2186

Protection against Electrophile and Oxidant Stress by Induction of the Phase 2 Response: Fate of Cysteines of the Keap1 Sensor Modified by Inducers. *Proc. Natl. Acad. Sci. U. S. A.* **2004**, *101*, 2040−2045.
(46) Hayes, J. D.; McMahon, M. The Double-Edged Sword of Nrf2: Subversion of Redox Homeostasis during the Evolution of Cancer. *Mol. Cell* **2006**, *21*, 732−734.
(47) Suzuki, T.; Maher, J.; Yamamoto, M. Select Heterozygous Keap1Mutations Have a Dominant-Negative Effect on Wild-Type Keap1 in vivo. *Cancer Res.* **2011**, *71*, 1700−1709.
(48) Singh, A.; Misra, V.; Thimmulappa, R. K.; Lee, H.; Ames, S.; Hoque, M. O.; Herman, J. G.; Baylin, S. B.; Sidransky, D.; Gabrielson, E.; Brock, M. V.; Biswal, S. Dysfunctional KEAP1-NRF2 Interaction in Non-Small-Cell Lung Cancer. *PLoS Med.* **2006**, *3*, e420.
(49) Lo, S. h.; Li, X.; Henzl, M. T.; Beamer, L. J.; Hannink, M. Structure of the Keap1: Nrf2 Interface Provides Mechanistic Insight into Nrf2 Signaling. *EMBO J.* **2006**, *25*, 3605−3617.
(50) Ichimura, Y.; Waguri, S.; Sou, Y.-s.; Kageyama, S.; Hasegawa, J.; Ishimura, R.; Saito, T.; Yang, Y.; Kouno, T.; Fukutomi, T.; Hoshii, T.; Hirao, A.; Takagi, K.; Mizushima, T.; Motohashi, H.; Lee, M.-S.; Yoshimori, T.; Tanaka, K.; Yamamoto, M.; Komatsu, M. Phosphorylation of p62 Activates the Keap1−Nrf2 Pathway during Selective Autophagy. *Mol. Cell* **2013**, *51*, 618−631.
(51) Li, X.; Zhang, D.; Hannink, M.; Beamer, L. J. Crystal Structure of the Kelch Domain of Human Keap1. *J. Biol. Chem.* **2004**, *279*, 54750−54758.
(52) Jorgensen, W. L.; Chandrasekhar, J.; Madura, J. D.; Impey, R. W.; Klein, M. L. Comparison of Simple Potential Functions for Simulating Liquid Water. *J. Chem. Phys.* **1983**, *79*, 926−935.
(53) Mark, P.; Nilsson, L. Structure and Dynamics of the TIP3P, SPC, and SPC/E Water Models at 298 K. *J. Phys. Chem. A* **2001**, *105*, 9954−9960.
(54) Hockney, R. W.; Eastwood, J. W. *Computer Simulation Using Particles*; McGraw-Hill: New York, 1981.
(55) Ryckaert, J.-P.; Ciccotti, G.; Berendsen, H. J. Numerical Integration of the Cartesian Equations of Motion of a System with Constraints: Molecular Dynamics of n-alkanes. *J. Comput. Phys.* **1977**, *23*, 327−341.
(56) Van Gunsteren, W.; Berendsen, H. Algorithms for Macromolecular Dynamics and Constraint Dynamics. *Mol. Phys.* **1977**, *34*, 1311−1327.
(57) Pearson, K. LIII. On lines and planes of closest fit to systems of points in space. *Philos. Mag. Ser. 6* **1901**, *2*, 559−572.
(58) Hotelling, H. Analysis of a Complex of Statistical Variables into Principal Components. *J. Educ. Psychol.* **1933**, *24*, 417.
(59) Bakan, A.; Bahar, I. Computational Generation Inhibitor-Bound Conformers of p38 MAP Kinase and Comparison with Experiments. In *Biocomputing 2011: Proceedings of the Pacific Symposium*; World Scientific: Singapore, 2011; pp 181−192.
(60) Bakan, A.; Bahar, I. The Intrinsic Dynamics of Enzymes Plays a Dominant Role in Determining the Structural Changes Induced upon Inhibitor Binding. *Proc. Natl. Acad. Sci. U. S. A.* **2009**, *106*, 14349−14354.
(61) Bakan, A.; Meireles, L. M.; Bahar, I. ProDy: Protein Dynamics Inferred from Theory and Experiments. *Bioinformatics* **2011**, *27*, 1575−1577.

DOI: 10.1021/acs.jcim.5b00300
J. Chem. Inf. Model. 2015, 55, 2178−2186